

# Monte Carlo Neural Operator for Learning PDEs via Probabilistic Representation

Rui Zhang<sup>\*a</sup>, Qi Meng<sup>†b</sup>, Rongchan Zhu<sup>c</sup>, Yue Wang<sup>b</sup>, Wenlei Shi<sup>b</sup>, Shihua Zhang<sup>a</sup>, Zhi-Ming Ma<sup>a</sup>, and Tie-Yan Liu<sup>b</sup>

<sup>a</sup>Academy of Mathematics and Systems Science, Chinese Academy of Sciences,  
Zhongguancun East Road, Beijing, China

<sup>b</sup>Microsoft Research, Danling Street, Haidian, Beijing, China

<sup>c</sup>Bielefeld University, Bielefeld, North Rhine-Westphalia, Germany

February 13, 2023

## Abstract

Neural operators, which use deep neural networks to approximate the solution mappings of partial differential equation (PDE) systems, are emerging as a new paradigm for PDE simulation. The neural operators could be trained in supervised or unsupervised ways, i.e., by using the generated data or the PDE information. The unsupervised training approach is essential when data generation is costly or the data is less qualified (e.g., insufficient and noisy). However, its performance and efficiency have plenty of room for improvement. To this end, we design a new loss function based on the Feynman-Kac formula and call the developed neural operator Monte-Carlo Neural Operator (MCNO), which can allow larger temporal steps and efficiently handle fractional diffusion operators. Our analyses show that MCNO has advantages in handling complex spatial conditions and larger temporal steps compared with other unsupervised methods. Furthermore, MCNO is more robust with the perturbation raised by the numerical scheme and operator approximation. Numerical experiments on the diffusion equation and Navier-Stokes equation show significant accuracy improvement compared with other unsupervised baselines, especially for the vibrated initial condition and long-time simulation settings.

## 1 Introduction

Diffusion is a common and important phenomenon in nature, which plays a significant role in science and engineering such as fluid mechanics [43], heat conduction [31], quantum mechanics [6]. From a macroscopic point of view, diffusion means the transport of mass from high concentration region to the low concentration one, which is mathematically described by the Laplacian operator [9] and widely appears in diffusion equation, Navier-Stokes equation, etc. To simulate the above physical processes, researchers have developed some well-known classical numerical methods for partial differential equations (PDEs), including Finite Difference Method (FDM), Finite Volume Method (FVM), Spectral Method (SM), etc [22].

---

<sup>\*</sup>This work was done when the author was visiting Microsoft Research.

<sup>†</sup>E-mails: rayzhang@amss.ac.cn, meq@microsoft.com

Besides the classical numerical methods, the so-called neural operators are emerging as a new paradigm for simulating PDE systems with the development of deep learning. In neural operator learning tasks, deep neural networks play a role as the approximators of the solution mapping (i.e., the mapping between the PDE’s parameters or conditions to the solution) for PDEs. Along this direction, several studies have proposed diverse network architectures for neural operators [3, 4, 26, 30]. These operators could be learned in both supervised [26, 30] and unsupervised ways [51, 54], using the pre-generated data or the PDE information to construct the training targets, respectively. The unsupervised way of training is essential for regularizing the deep learning model, especially for the scenario where generated data is not qualified. However, it still lacks a thorough study on unsupervised loss design in learning the neural operator, which makes its training less efficient (e.g., it requires fine-grained residual terms and cannot simulate for a long time) compared with the supervised approach.

In this work, we propose a novel unsupervised way to train the neural operator for a class of PDE systems with diffusion. It is motivated by the microscopic view of the diffusion, i.e., the ensemble of the random movements of microscopic particles [57]. Therefore, the solutions of a PDE system with diffusion allow probabilistic representation, which is easily simulated via Monte Carlo approximation. Leveraging the probabilistic representation, we develop Monte Carlo Neural Operator (MCNO), a novel way to train the neural operator in an unsupervised manner. It inherits the advantages from Monte Carlo-based methods (MCM), including robustness for larger temporal steps and efficiency in handling fractional diffusion operators.

We conduct in-depth analyses on the performance of MCNO both theoretically and experimentally. In theory, we characterize the approximation error and the robustness of MCNO with respect to the vibration of the spatial condition, the temporal discretization scheme, and the diffusive coefficients. Numerical results show that MCNO has significant benefits compared to FDM-based methods, especially for simulating tasks requiring complex spatial conditions and larger temporal steps. Our experiments on the diffusion equation, Burgers’ equation, and Navier-Stokes equation could support our theoretical claim. Besides, our work is the first time to simulate these equations for a long period in an unsupervised approach with large steps, e.g., simulating the Navier-Stokes equation for 5s with  $\Delta t = 0.5s$ , which is super challenging for existing unsupervised loss. In summary, we make the following contributions:

1. We propose MCNO, a new Monte Carlo-based unsupervised approach to train the neural operator for a class of PDE systems with diffusion, which is robust for spatial-temporal variation and efficient for handling fractional operators.
2. We prove that MCNO has accuracy and robustness benefits compared to FDM-based methods, especially for problems with complex spatial conditions and larger temporal steps. Furthermore, the stochastic label noise from the Monte Carlo sampling could help generalization when handling the diffusion terms, while the deterministic bias in other unsupervised training signals is harmful in general.
3. The experiments on the diffusion equation and Navier-Stokes equation show significant improvements in accuracy compared with other unsupervised neural operators. Moreover, it is the first time for a neural operator to simulate turbulent flows for a long period in an unsupervised approach with large steps.

## 2 Related Works

**Neural Operators** Neural operators are proposed to learn a mapping between the infinite-dimensional function spaces, e.g., the mapping between PDE’s initial condition or force term

(sampled from a distribution) to its solution [30]. [30] proposed DeepONet to encode the initialization conditions and queried locations via branch and trunk nets, respectively. [23] and [25] learn the operator in Fourier space via Fast Fourier Transform, which can handle different frequency components efficiently. Moreover, several works utilize graph neural networks [3, 26] or transformers [4, 24] as the surrogate models between functional spaces. However, the above methods require the supervision of ground-truth data generated via accurate numerical solvers, which is quite time-consuming in general. To this end, some neural operators aim to train the operator without the supervision of data [15, 28, 51, 54]. [54] proposed PI-DeepONets, which utilize the PDE residuals to train DeepONets in an unsupervised way. [15] proposed Meta-Auto-Decoder, a meta-learning approach to learn families of PDEs in the unsupervised regime. Furthermore, [51] and [28] utilize the residuals of the FDM to train the neural operators. Compared with these unsupervised methods, MCNO encodes the physics information via Feynman-Kac law, which can allow larger roll-out steps and efficiently handle (fractional) Laplacian terms.

**Physics-Informed Neural Networks (PINNs)** PINNs are proposed to solve the PDE system by using the residual of the PDE to approximate its solution (i.e., the point-to-point mapping between the spatial-temporal point to the solution value). They are widely used to solve a specific PDE or the inverse problems [5, 18, 44, 61]. Recently, PINNs have obtained significant progress in solving scientific problems based on the PDEs, including Navier-Stokes equations [16, 33, 45], Schrödinger equations [14, 23], Allen Cahn equations [17, 34], and so on. Apart from constructing the loss function via the PDE residuals directly, some works also utilize the probabilistic representation of PDEs to train neural networks [11, 13, 58], which can handle high dimensional or fractional PDEs efficiently [11, 12, 46, 47]. Furthermore, some studies design the loss functions based on other numerical methods, including finite volume method [1], finite element method [36, 38], energy-based method [56], etc. It is worth mentioning that the above PINN methods have to retrain the neural networks when meeting a PDE with changed conditions (e.g., initial conditions), which is time-consuming. In this paper, we aim to learn operators between infinite dimensional spaces, which can generalize to different conditions of the PDEs over a distribution, and then, we could simulate different PDE instances simultaneously without additional training costs.

## 3 Methodology

### 3.1 Preliminary

In this paper, we consider a class of PDEs with a linear term given by the Laplacian operator defined as follows:

$$\frac{\partial u}{\partial t} = \beta[u](\mathbf{x}, t) \cdot \nabla u + \kappa \Delta u + f(\mathbf{x}, t), \quad (1)$$

$$u(\mathbf{x}, 0) = u_0(\mathbf{x}), \quad (2)$$

where  $\mathbf{x} \in \Omega \subset \mathbb{R}^d$ ,  $t$  denotes the  $d$ -dimensional spatial variable and the time variable, respectively,  $u : \Omega \times (0, T] \rightarrow \mathbb{R}$ ,  $\beta[u](\mathbf{x}, t) \in \mathbb{R}^d$  is a vector-valued mapping from  $u$  to  $\mathbb{R}^d$ ,  $\kappa \in \mathbb{R}^+$  is the diffusion parameter, and  $f(\mathbf{x}, t) \in \mathbb{R}$  denotes the force term. Given the initial condition  $u_0(\mathbf{x})$ , we are interested in the evolution of  $u_t(\mathbf{x})$  for  $t \in (0, T]$ . Many well-known PDEs can be viewed as a special form of Eq. 1, such as diffusion equations, Burgers' equation, etc.

For such PDEs with the form as Eq. 1, the Feynman-Kac formula provides the relationship between the PDEs and corresponding probabilistic representation [12, 39, 40]. In detail, we can

use the time inversion (i.e.,  $\tilde{u}(\mathbf{x}, t) = u(\mathbf{x}, T - t)$ ,  $\tilde{f}(\mathbf{x}, t) = f(\mathbf{x}, T - t)$ ) to the PDE as:

$$\frac{\partial \tilde{u}}{\partial t} = -\beta[\tilde{u}](\mathbf{x}, t) \cdot \nabla \tilde{u} - \kappa \Delta \tilde{u} - \tilde{f}(\mathbf{x}, t), \quad (3)$$

$$\tilde{u}(\mathbf{x}, T) = u_0(\mathbf{x}). \quad (4)$$

Applying the Feynman–Kac formula [32] to the terminal value problem Eq. 3, we have

$$\tilde{u}_0(\mathbf{x}) = \mathbb{E}_{\boldsymbol{\xi}} \left[ \tilde{u}_T(\boldsymbol{\xi}_T) + \int_0^T \tilde{f}(\boldsymbol{\xi}_s, s) ds \right], \quad (5)$$

where  $\boldsymbol{\xi}_s \in \mathbb{R}^d$  is a random process starting at  $\mathbf{x}$ , and moving from 0 to  $T$ , which satisfies:

$$\begin{aligned} d\boldsymbol{\xi}_t &= \beta[\tilde{u}](\boldsymbol{\xi}_t, t) dt + \sqrt{2\kappa} d\mathbf{B}_s, \\ \boldsymbol{\xi}_0 &= \mathbf{x}, \end{aligned} \quad (6)$$

where  $\mathbf{B}_s$  is the  $d$ -dimensional standard Brownian motion. Applying time inversion  $t \rightarrow T - t$  to Eq. 5, we have

$$u_T(\mathbf{x}) = \mathbb{E}_{\boldsymbol{\xi}} \left[ u_0(\boldsymbol{\xi}_T) + \int_0^T f(\boldsymbol{\xi}_s, T - s) ds \right]. \quad (7)$$

### 3.2 Monte Carlo Neural Operator

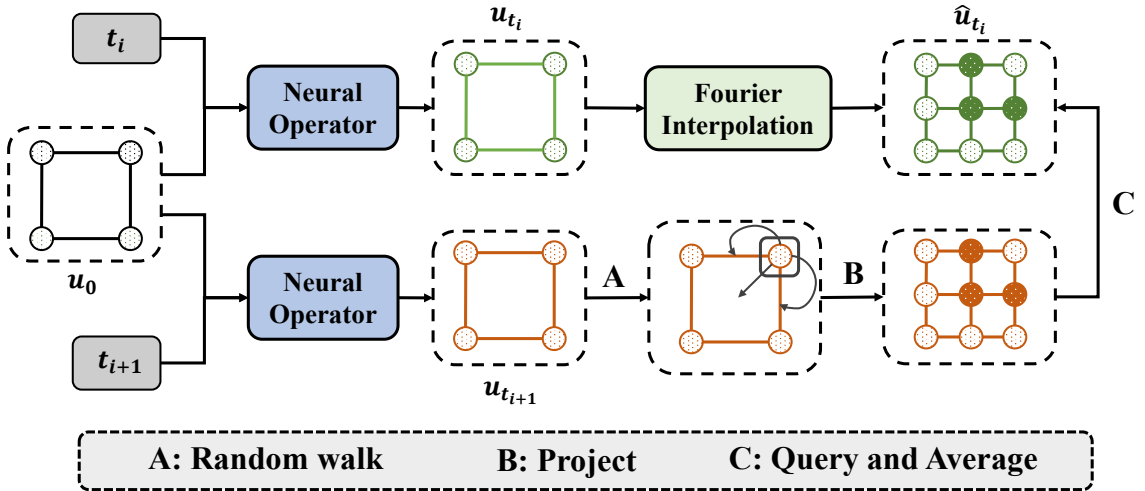


Figure 1: **Illustration of the training process of MCNO.** We construct the training loss via the relationship between  $u_{t_i}$  and  $u_{t_{i+1}}$  given by the Feynman-Kac law. **A:** random walk according to the stochastic process in Eq. 11, and denote the  $M$  particles starting at the grid point  $\mathbf{x}$  as  $\{\tilde{\boldsymbol{\xi}}_t^m\}_{m=1}^M$ ; **B:** project each  $\tilde{\boldsymbol{\xi}}_t^m$  to the nearest coordinate point  $\hat{\boldsymbol{\xi}}_t^m$  in the high resolution coordinate system; **C:** query the value of each  $\hat{\boldsymbol{\xi}}_t^m$  via  $\hat{u}_{t_i}$  and average  $\hat{u}_{t_i}(\hat{\boldsymbol{\xi}}_t^m)$ , and note that the high-resolution  $\hat{u}_{t_i}$  is obtained from  $u_{t_i}$  via Fourier interpolation. Then, the loss function of MCNO at  $\mathbf{x}$  is given by:  $\|\mathcal{G}_\theta(u_0, t_{i+1})(\mathbf{x}) - \sum_{m=1}^M \hat{u}_{t_i}(\hat{\boldsymbol{\xi}}_t^m)\|_2^2$ .

Given a PDE with the form of Eq. 1 and a distribution of the initial conditions  $\mathcal{D}_0$ , the target of MCNO is to learn a functional mapping  $\mathcal{G}_\theta$  with parameter  $\theta$  which can simulate the

subsequent fields for all initial fields  $u_0 \sim \mathcal{D}_0$  at time  $t \in [0, T]$ . In detail, the inputs and outputs of  $\mathcal{G}_\theta$  are given as follows:

$$\begin{aligned} \mathcal{G}_\theta : \mathcal{D}_0 \times (0, T] &\rightarrow \mathcal{D}_{(0, T]}, \\ (u_0, t) &\mapsto u_t, \end{aligned} \quad (8)$$

where  $\mathcal{D}_{(0, T]}$  denotes the joint distribution of the field after  $t = 0$ . Unlike other supervised operator learning algorithms [3, 23, 30], MCNO aims to learn the operator in an unsupervised way, i.e., only utilize the physics information provided by PDEs. To this end, MCNO considers training the operator in a pure PDE equation driven approach via the relationship between  $u_{t_i}$  and  $u_{t_{i+1}}$  (where  $0 = t_0 < \dots < t_i < t_{i+1} < \dots < t_m = T$ ) derived by the aforementioned probabilistic representation. Considering Eq. 7, an expected neural operator  $\mathcal{G}_\theta$  should satisfy the following equation:

$$\mathcal{G}_\theta(u_0, t_{i+1})(\mathbf{x}) = \mathbb{E}_\xi [\mathcal{G}_\theta(u_0, t_i)(\xi_{t_{i+1}}) + \int_{t_i}^{t_{i+1}} f(\xi_s, t_i + (t_{i+1} - s)) ds], \quad (9)$$

where  $\xi_s (s \in (t_i, t_{i+1}])$  is generated by Eq. 6 with  $\xi_{t_i} = \mathbf{x}$ .

Regarding Eq. 9 as the optimization objective, the expected loss function of MCNO can be written as follows:

$$\mathcal{L}_{\text{MCNO}} = \sum_{i=0}^{m-1} \mathbb{E}_{u_0} [\|\mathcal{G}_\theta(u_0, t_{i+1})(\mathbf{x}) - \mathbb{E}_\xi [\mathcal{G}_\theta(u_0, t_i)(\xi_{t_{i+1}}) + \int_{t_i}^{t_{i+1}} f(\xi_s, t_i + t_{i+1} - s) ds]\|_2^2], \quad (10)$$

where  $\mathcal{G}_\theta(u_0, t_0)$  is directly set to be  $u_0$  in experiments.

Equipped with the loss function Eq. 10, we sample the initial states  $u_0$  from  $\mathcal{D}_0$  uniformly for each epoch, calculate the Monte Carlo loss  $\mathcal{L}_{\text{MCNO}}$ , and utilize Adam [19] to optimize the neural operator  $\mathcal{G}_\theta$  until converge. Here, we use the Monte Carlo method to estimate the expectation with respect to  $u_0$  and  $\xi$ , and details will be introduced as below.

### 3.3 Implementation Details of MCNO

In this section, we introduce some important implementation details for MCNO. We illustrate the framework and training process of MCNO in Fig. 1 and the overall algorithm in Appendix A.

**Spatial Discretization** In this paper, we are interested in the evolution of PDEs at fixed grids  $\{\mathbf{x}_p\}_{p=1}^P \in \Omega$ .<sup>1</sup> Accordingly, the inputs and outputs of the operator  $\mathcal{G}_\theta$  are equation values at  $P$  coordinate points, respectively. Thus, when calculating the loss function between  $\mathcal{G}_\theta(u_0, t_i)$  and  $\mathcal{G}_\theta(u_0, t_{i+1})$ , the particles start from each grid point  $\mathbf{x}_p$  at time  $t_{i+1}$ , respectively, and then walk back to time  $t_i$  according to the random process in Eq. 5.

**Temporal Discretization** When simulating the stochastic process in Eq. 6, we first apply time inversion and then mainly utilize the classical Euler–Maruyama method [53] to approximate the SDEs. In detail, the discrete formula for the SDE after applying time inversion to Eq. 6 is given as follows:

$$\begin{aligned} \tilde{\xi}_{t_i} &= \tilde{\xi}_{t_{i+1}} - \beta[u](\mathbf{x}, t_{i+1})\Delta t - \sqrt{2\kappa}\Delta \mathbf{B}_t, \\ \tilde{\xi}_{t_{i+1}} &= \mathbf{x}, \end{aligned} \quad (11)$$

<sup>1</sup>Here, we apply MCNO on fixed grids for ease of evaluation, although the Monte Carlo approach could be mesh-free and does not rely on specific grids.

where  $\tilde{\xi}$  is the time inversion process of  $\xi$  in time interval  $[t_i, t_{i+1}]$ , i.e.,  $\xi_{t_i+s}$  and  $\tilde{\xi}_{t_{i+1}-s}$  for  $s \in [0, t_{i+1} - t_i]$  have the same distribution. Please note that we apply a one-step roll-out at each time interval, i.e., at each  $t_{i+1}$ , MCNO generates the particles anew from  $x$ , and moves them back to  $t_i$  according to Eq. 11. The stochastic integral of the force  $f$  in Eq. 9 is approximated via Euler’s method, which is in line with [12]. Moreover, to handle some PDEs with large spatial-temporal variation, we also consider other numerical methods to simulate Eq. 6, including Runge–Kutta method [48] and Heun’s method [53]. More details are shown in Sec. 5.4.

**Random Walks** Eq. 5 and Eq. 6 describe the random walks driven by BSDEs of corresponding PDEs. For PDEs with periodical boundary conditions, particles should be pulled back according to the periodical law when walking out of the domain  $\Omega$ . For Dirichlet boundary conditions, the random walk of particles should stop once they reach the boundary. Furthermore, for PDEs with the fractional Laplacian  $-(-\Delta)^\alpha u$ , where  $\alpha \in (0, 2)$ , we only need to replace the Brownian motion with the  $\alpha$ -stable Lévy process [20, 59, 60].

**Fourier Interpolation Tricks** In Eq. 11, the free particles  $\tilde{\xi}_{t_i}$  need to query the value of  $\mathcal{G}_\theta(u_0, t_i)$  when approximating  $\mathcal{G}_\theta(u_0, t_{i+1})$ . To obtain the querying results efficiently, we project the particles  $\tilde{\xi}_{t_i}$  to the nearest grids in practice. To reduce projection errors as possible, we utilize the Fourier transform to interpolate the grid of  $u_{t_i} = \mathcal{G}_\theta(u_0, t_i)$  to the high-resolution one  $\hat{u}_{t_i}$  before the querying.

## 4 Theoretical Results

In this section, we study the theoretical properties of MCNO when simulating the diffusion equation, and the proofs can be seen in Appendix B. In detail, we consider the periodical diffusion equation<sup>2</sup> defined as follows:

$$\frac{\partial u}{\partial t} = \kappa \Delta u, \quad x \in [0, 2\pi], t \in [0, T]. \quad (12)$$

In Theorem 4.1, given the ground-truth  $u_t$ , we estimate the one-step error of predicted  $u_{t+\Delta t}$  constructed via FDM and MCM. Note that FDM is the source of training loss of PINO [28] and LordNet [51], while MCM is the one of MCNO. Considering that PINO utilizes the spectral method to calculate the spatial derivative, we ignore the error of the spatial derivative of FDM in the proof.

**Theorem 4.1.** *Let  $u_t(x)$  be the diffusion equation in the form of Eq. 12,  $u_{t+\Delta t}^{\text{FDM}}(x)$  and  $u_{t+\Delta t}^{\text{MCM}}(x)$  denote the one-step label starting from  $u_t(x)$ , given by FDM and MCM, respectively. Let  $L_a^b$  denote the Lipschitz coefficient of function  $a$  with respect to variable  $b$ . Then, we have*

- 1)  $|u_{t+\Delta t}^{\text{FDM}}(x) - u_{t+\Delta t}(x)| \leq \frac{\kappa L_{\Delta u}^t \Delta t^2}{2};$
- 2)  $|u_{t+\Delta t}^{\text{MCM}}(x) - u_{t+\Delta t}(x)| \leq \epsilon$  holds with probability at least  $1 - \frac{(2L_u^x)^2 \kappa \Delta t}{M\epsilon^2}.$

In Theorem 4.1, we compare the one-step roll-out error of MCM and FDM, respectively. However, when training neural operators, the discretization and approximation error, which are raised by the numerical method and the operator learning, will bring the inevitable error to  $u_t$ . To this end, we study the robustness of the target label conducted by FDM and MCM in Theorem 4.2.

<sup>2</sup>Additional analyses for Eq. 1 can be seen in Appendix B.1.

**Theorem 4.2.** Let  $u_t(x)$  be the diffusion equation in the form of Eq. 12, and assume the exact solution can be written as:  $u_t(x) = \sum_{n=1}^N \sin(nx)\phi_n(t)$ . Let  $\mathcal{G}_\theta$  be the neural operator, and its prediction on  $u_t(x)$  can be written as  $\mathcal{G}_\theta(u_0, t)(x) = \sum_{n=1}^N \sin(nx)(\phi_n(t) + r_n)$ , where  $r_n$  denotes the residual of coefficient on each Fourier basis. Let  $u_{t+\Delta t}^{\text{FDM}}(x)$  and  $u_{t+\Delta t}^{\text{MCM}}(x)$  denote the one-step label starting from  $\mathcal{G}_\theta(u_0, t)(x)$ , given by FDM and MCM, respectively. Then, we have

$$\begin{aligned} 1) & |u_{t+\Delta t}^{\text{FDM}}(x) - u_{t+\Delta t}(x)| \leq \sum_{n=1}^N |r_n(\kappa n^2 \Delta t - 1)| + o(\Delta t); \\ 2) & |u_{t+\Delta t}^{\text{MCM}}(x) - u_{t+\Delta t}(x)| \leq \sum_{n=1}^N |r_n| + \epsilon \text{ holds with probability at least } 1 - 2 \exp\left(-\frac{\epsilon^2 M}{2(\sum_{n=1}^N |\phi_n(t)|)^2}\right). \end{aligned}$$

**MCNO is robust with larger steps and spatial variation.** Theorem 4.1 reveals that the target of MCNO is unbiased when solving diffusion equations even with arbitrarily large temporal steps, and the variance can be reduced via the number of sampling. Furthermore, as shown in Theorem 4.2, the error caused by the residual  $r_n$  will be enlarged with the growth of  $n$  and  $\Delta t$  for FDM loss while holding steady for the MCM loss. This observation indicates that MCNO is robust with the small perturbation and can allow large roll-out steps during the training process compared to other FDM-based neural operators.

**The label noise in MCNO could help generalization.** In MCNO, the label to train the neural network is noisy. For example, the Monte Carlo realization (i.e.,  $\frac{1}{M} \sum_{m=1}^M \sqrt{2\kappa\Delta t} z_m$ ,  $z_m \sim N(0, 1)$ ) of the term  $\int_t^{t+\Delta t} \sqrt{2\kappa} dB_s$  introduces the label noise in the training objective of MCNO for diffusion equations. Some studies show that label noise could regularize the optimization trajectory of the optimizer and help generalization in deep learning [8]. Thus, the label noise from the Monte Carlo sampling could help generalization when handling the diffusion terms. At the same time, the deterministic bias in other unsupervised training signals is harmful in general. It is another advantage of MCNO compared with FDM-based operators (e.g., PINO), which is also verified by the experiments.

## 5 Experiments

In this section, we conduct numerical experiments to evaluate the proposed MCNO on the following four tasks, including 1D (fractional) diffusion equations, 2D Navier-Stokes equations, 1D Burgers' equation, and heat diffusion on a circular ring. The implementation details of MCNO and other baseline methods are introduced in Appendix C. The ablation experiments can be seen in Appendix C.3. We evaluate the model performances for all tasks via the relative  $\ell_2$  error on 100 test PDE samples. We repeat each experiment with three random seeds and report the mean value and variance. All experiments are implemented on NVIDIA A100 GPU.

### 5.1 1D Diffusion Equation

In this section, we conduct experiments on periodical 1D diffusion equation defined as follows:

$$\frac{\partial u(x, t)}{\partial t} = -\kappa(-\Delta)^{\frac{\alpha}{2}} u(x, t), \quad x \in [0, 1], t \in [0, T], \quad (13)$$

where the diffusion parameter  $\alpha$  is restricted to the interval  $(0, 2]$ . Notice that  $\alpha = 2$  represents the original Laplacian operator, while  $\alpha \in (0, 2)$  denotes the fractional operator, which is defined by directional derivatives [29, 37].

We generate the initial states  $u(x, 0)$  from the following functional space  $\mathcal{F}_N$ :

$$\mathcal{F}_N \triangleq \left\{ \sum_{n=1}^N a_n \sin(2\pi nx) : a_n \sim \mathcal{U}(0, 1) \right\}, \quad (14)$$

where  $\mathcal{U}(0, 1)$  denotes the uniform distribution over  $(0, 1)$ , and  $N$  represents the maximum frequency of the functional space. In this case, we can obtain the exact solution for both the original and fractional diffusion equations as follows:

$$u(x, t) = \sum_{n=1}^N a_n \sin(2\pi nx) e^{-\kappa(2\pi n)^\alpha t}. \quad (15)$$

Specially, we consider the following three problem settings, including short temporal simulation with different  $N$ , long temporal simulation with different  $\kappa$ , and fractional Laplacian simulation with different  $\alpha$ . For all the above experiments, we divide the domain  $[0, 1]$  into 64 grid elements. When conducting MCNO, we divide the time horizon into 2 (10) steps for short (long) simulation, respectively. We fix the time step of PINO as 100 in all experiments.

### 5.1.1 Short temporal simulation

In this case, we aim to evaluate the robustness of the proposed methods to the maximum frequency of the functional space. We choose  $T = 1s$ ,  $\kappa = 10^{-3}$  and  $\alpha = 2$ . We conduct five experiments with  $N = \{2, 4, 6, 8, 10\}$ , respectively. Fig. 2 displays the exact versus predicted  $u$  of MCNO at  $t = 1.0s$  with  $N = 2$  and 10, respectively. The results in Table 1 show that MCNO is the most accurate and robust method when handling initial conditions with various frequencies, which is in line with Theorems 4.1 and 4.2. Moreover, the relative error of PI-DeepONet increases rapidly as  $N$  increases, which indicates that the PINN loss cannot deal with high-frequency components efficiently. Similarly, this phenomenon has also been observed in the previous literature [21, 55]. Furthermore, thanks to the large time steps, the training speed of MCNO is obviously fast than other baseline methods (Table 1).

Table 1: Short temporal simulation of 1D diffusion equation with  $T = 1s$  and  $\kappa = 10^{-3}$ . Relative errors (%) and computational costs for three methods with  $N = \{2, 4, 6, 8, 10\}$ , respectively.

	PI-DEEPONET	PINO	MCNO
ERROR ( $N = 2$ )	0.34± 0.05	0.30± 0.01	0.27± 0.03
ERROR ( $N = 4$ )	0.58± 0.09	0.50± 0.09	0.14± 0.01
ERROR ( $N = 6$ )	1.53± 0.06	0.64± 0.23	0.19± 0.01
ERROR ( $N = 8$ )	8.24± 2.07	1.31± 0.41	0.25± 0.02
ERROR ( $N = 10$ )	28.55± 5.39	1.94± 0.58	0.30± 0.03
TIME (INFER, MS)	1.81	2.09	1.75
TIME (TRAIN, H)	2.42	1.17	0.12
PARAMETERS	152700	3289537	36577

### 5.1.2 Long Time Simulation

In this case, we aim to simulate the diffusion equation with  $\kappa = 10^{-2}$  and  $10^{-3}$ , respectively. We set  $T = 5s$ ,  $\alpha = 2$  and  $N = 10$ . The main difficulty of this task is the long time prediction, and it is worth mentioning that the case  $\kappa = 10^{-2}$  is even more difficult due to the exponential decay rate in Eq. 15. Compared with other methods, only MCNO achieves relatively low error when  $\kappa = 10^{-2}$  (Table 2). We also evaluate the performance of FDM when  $\kappa = 10^{-2}$  and observe that the results of FDM blow up when the number of steps is fixed as 100 ( $10\times$  fine compared with MCNO). Such observation explains why PINO fails on the task when  $\kappa = 10^{-2}$ .



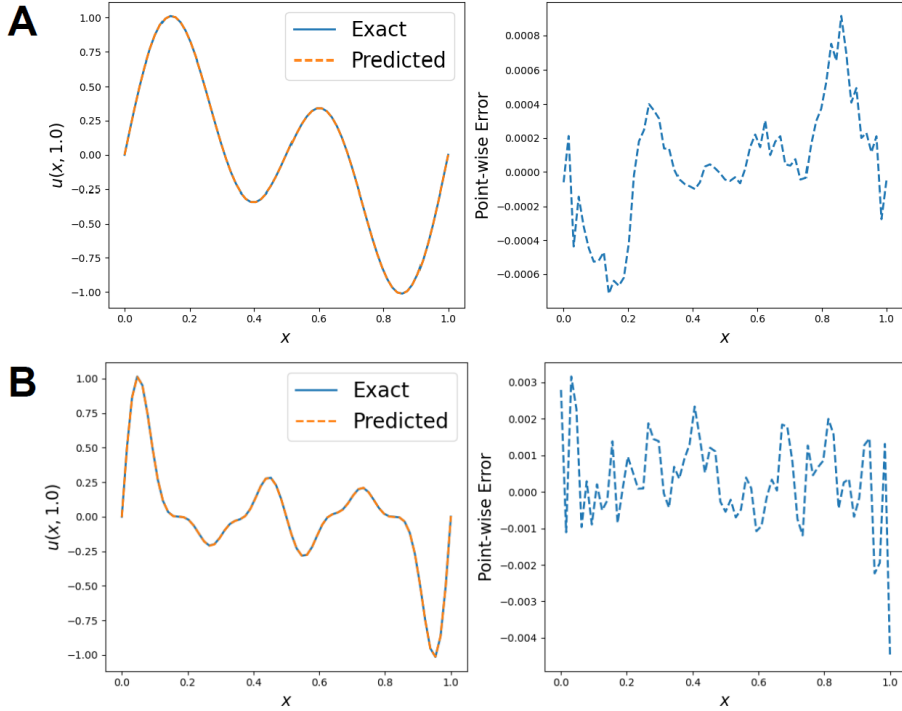


Figure 2: Short temporal simulation of 1D diffusion equation with  $N = 2$  (A) and  $N = 10$  (B) at  $t = 1.0s$ , respectively. Exact solution versus the prediction of a learned MCNO for an example in the test set.

Table 2: Long temporal simulation of 1D diffusion equation with  $T = 5s$  and  $N = 10$ . Relative errors (%) and computational costs for three methods on  $\kappa = 10^{-2}$  and  $10^{-3}$ .

	PI-DEEPONET	PINO	MCNO
ERROR ( $\kappa = 10^{-2}$ )	152.51± 38.21	7.89± 2.83	1.61± 0.20
ERROR ( $\kappa = 10^{-3}$ )	28.10± 2.71	1.73± 0.44	0.60± 0.16
TIME (INFER, MS)	1.86	2.09	1.78
TIME (TRAIN, H)	2.42	1.17	0.57
PARAMETERS	152700	3289537	36577

### 5.1.3 Fractional Laplacian Simulation

In this case, we aim to show the ability of MCNO when handling the fractional diffusion equation. We choose the diffusion parameter  $\alpha = 0.5$  and  $1$ , respectively. We set  $T = 5s$ ,  $\kappa = 10^{-3}$  and  $N = 10$ . Since other physics-driven operator learning methods do not consider the fractional operators, here we compare MCNO with the traditional numerical method MCM instead. For the task  $\alpha = 1.0$ , the accuracy of MCM cannot reach MCNO even if the number of sampling comes up to  $1.5 \times 10^4$  (Fig. 3). For the task  $\alpha = 0.5$ , the performance of MCM outperforms MCNO when the number of sampling is  $10^4$ , which will take  $700\times$  inference time compared with

MCNO<sup>3</sup>. Note that the case  $\alpha = 0.5$  takes more inference time for MCM compared with  $\alpha = 1.0$  due to the random walk governed by the Lévy process of  $\alpha = 0.5$  needs more computational costs.

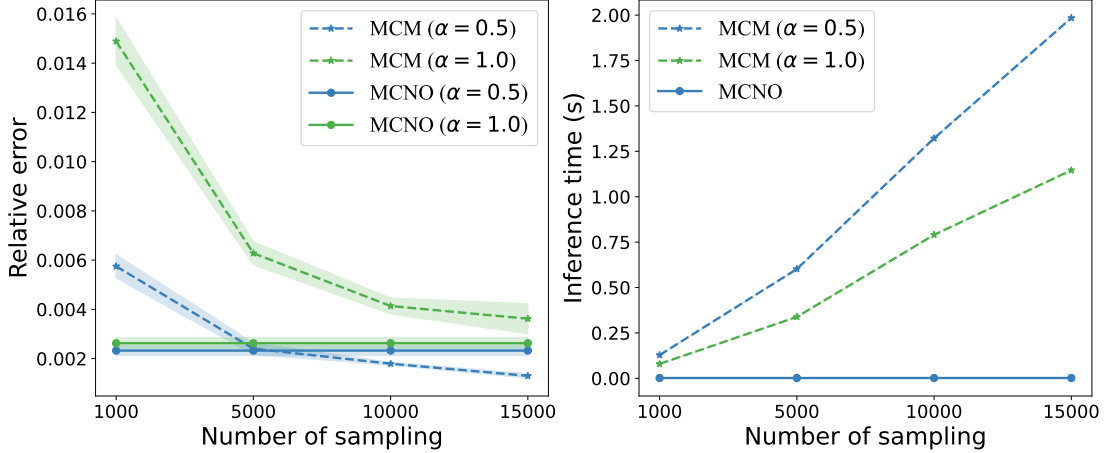


Figure 3: Fractional Laplacian simulation of 1D diffusion equation with  $N = 10$  and  $\kappa = 10^{-3}$ . **Left:** The dashed lines represent the relative errors (%) of MCM with different numbers of sampling, and the solid ones denote the error of the trained MCNO. **Right:** The inference time for MCNO and MCM evaluated on one sample in the test set, respectively.

## 5.2 2D Navier-Stokes Equation

In this experiment, we simulate the velocity field for 2D flows in a periodic domain  $\Omega = [0, 1] \times [0, 1]$  without (or with) an external force, whose vortex equation is given as follows:

$$\begin{aligned} \frac{\partial \omega}{\partial t} &= -(\mathbf{u} \cdot \nabla) \omega + \nu \Delta \omega + f(\mathbf{x}), \\ \omega &= \nabla \times \mathbf{u}, \end{aligned} \quad (16)$$

where  $f(\mathbf{x})$  is the forcing function, and  $\nu \in \mathbb{R}^+$  represents the viscosity term. We choose the viscosity terms in  $\{10^{-3}, 10^{-4}, 10^{-5}\}$  to simulate different flows, and the initial vorticity is generated from the Gaussian random field  $\mathcal{N}(0, 7^{3/2}(-\Delta + 49\mathbf{I})^{-2.5})$  with periodic boundaries. We divide the domain  $\Omega$  into  $64 \times 64$  grid elements. The time horizon  $[0, 5]$  is divided into 10 (100) uniform intervals for MCNO (PINO), respectively.

### 5.2.1 Without an External Force

In this experiment, the external force  $f(\mathbf{x})$  is fixed as zero. As shown in Table 3, MCNO outperforms PINO for all tasks, and the advantages become more prominent when  $\nu = 10^{-5}$ . Moreover, when the viscosity term  $\nu$  decreases, it is harder to simulate the flow because it is getting more turbulent, which agrees with the law of physics. Fig. 4 displays the ground-truth versus predicted  $\omega$  of MCNO at  $t = 5.0s$  with  $\nu = 10^{-3}$  and  $10^{-5}$ , respectively. It can be seen that the vorticity fields become more complicated when  $\nu = 10^{-5}$ ; thus, the corresponding task

<sup>3</sup>Some implementation details can be seen in Appendix C.2.1

will become more challenging. It is also worth mentioning that we only discrete the time horizon  $[0, 5]$  into ten steps for MCNO, which is ten times coarser when conducting PINO. This reveals the ability of MCNO to adapt to large roll-out steps during the training process.

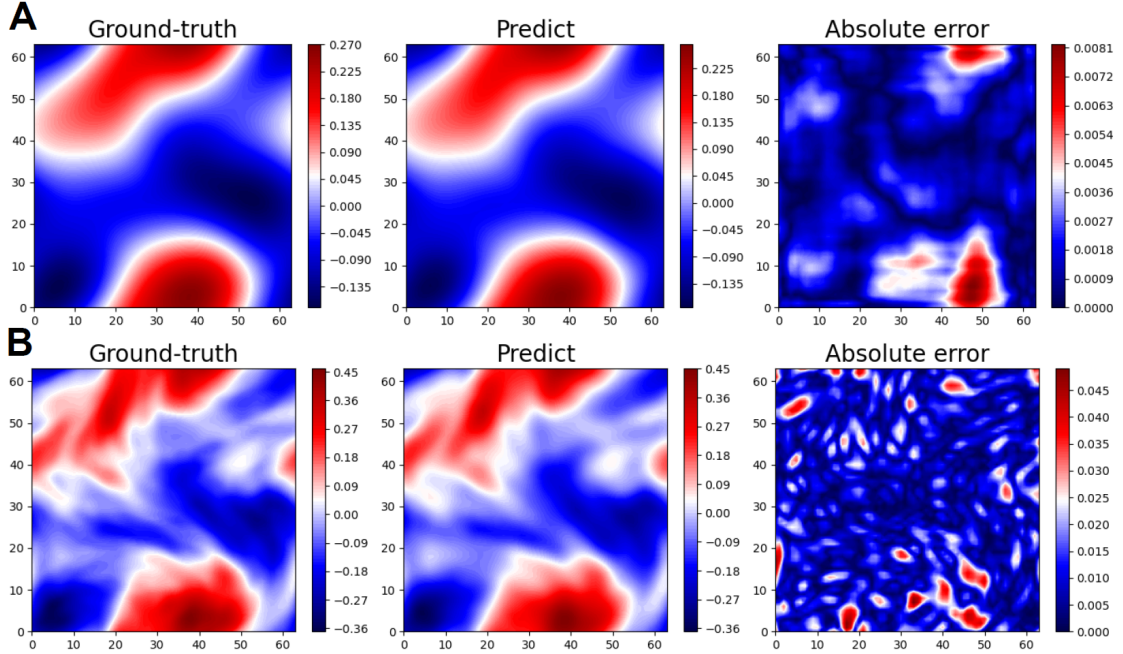


Figure 4: Simulation of 2D Navier-Stokes equations without an external force. The ground-truth solution versus the prediction of a learned MCNO for an example in the test set at  $t = 5.0s$ , with the viscosity terms  $\nu = 10^{-3}$  (**A**) and  $\nu = 10^{-5}$  (**B**), respectively.

Table 3: 2D Navier-Stokes equations simulation without an external force. Relative errors (%) and computational costs for PINO and MCNO with  $\nu = \{10^{-3}, 10^{-4}, 10^{-5}\}$ , respectively.

	PINO	MCNO
ERROR ( $\nu = 10^{-3}$ )	$2.42 \pm 0.27$	$2.03 \pm 0.32$
ERROR ( $\nu = 10^{-4}$ )	$5.28 \pm 0.21$	$4.31 \pm 0.21$
ERROR ( $\nu = 10^{-5}$ )	$9.34 \pm 0.29$	$6.16 \pm 0.12$
TIME (INFER, MS)	4.53	4.53
TIME (TRAIN, H)	6.17	1.08
PARAMETERS	1481009	1481009

### 5.2.2 With an External Force

In this case, we consider the Navier-Stokes equations with an external force  $f(\mathbf{x})$ , which is defined as follows [23]:

$$f(\mathbf{x}) = 0.1 \sin(2\pi(\mathbf{x}_1 + \mathbf{x}_2)) + 0.1 \cos(2\pi(\mathbf{x}_1 + \mathbf{x}_2)).$$

Table 4: 2D Navier-Stokes equations simulation with an external force. Relative errors (%) and computational costs for PINO and MCNO with  $\nu = \{10^{-3}, 10^{-4}, 10^{-5}\}$ , respectively.

	PINO	MCNO
ERROR ( $\nu = 10^{-3}$ )	$3.00 \pm 0.16$	$3.47 \pm 0.41$
ERROR ( $\nu = 10^{-4}$ )	$8.52 \pm 0.30$	$5.25 \pm 0.30$
ERROR ( $\nu = 10^{-5}$ )	$11.11 \pm 0.36$	$6.57 \pm 0.22$
TIME (INFER, MS)	4.53	4.53
TIME (TRAIN, H)	6.17	1.08
PARAMETERS	1481009	1481009

As shown in Table 4, MCNO outperforms PINO for the tasks  $\nu = 10^{-4}$  and  $10^{-5}$ , and the corresponding gaps between MCNO and PINO get wider when the force term is involved.

### 5.3 Heat Diffusion on a Circular Ring

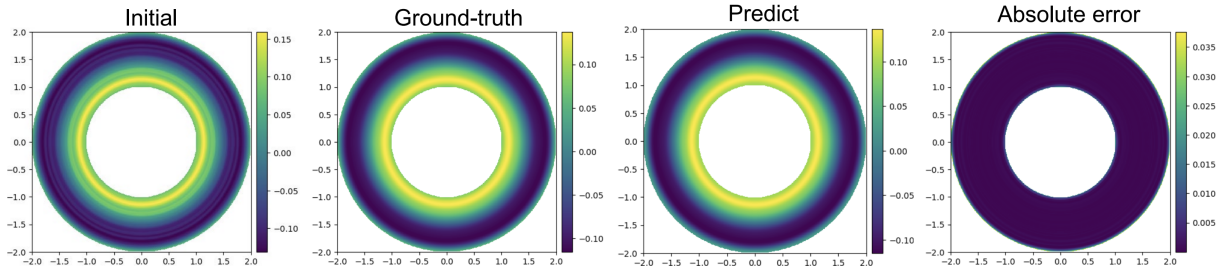


Figure 5: Simulation of heat diffusion on a circular ring (Eq. 17). The ground-truth solution versus the prediction of a learned MCNO for an example in the test set at  $t = 1.0s$ .

In this experiment, we utilize MCNO to simulate the heat equation on a circular ring, which aims to reveal how MCNO handles such irregular boundaries with Dirichlet conditions. The center of the ring located at the origin and the radiuses of the two circles are equal to 1 and 2, respectively (Fig. 5). In detail, the PDE is defined as follows:

$$\frac{\partial u(\mathbf{x}, t)}{\partial t} = 0.001 \Delta u(\mathbf{x}, t), \quad (17)$$

where  $1 < \|\mathbf{x}\|_2^2 < 2, t \in [0, 1]$ .

For such tasks with Dirichlet boundary, the random walks of particles need to stop when reaching the boundary. The initial conditions are set to the spherically symmetric regime; thus, we only need to consider the value of PDEs at  $\{(\mathbf{x}_1, 0) : \mathbf{x}_1 \in [1, 2]\}$ , while the random walks of particles are simulated in the 2D space. The simulation of MCNO is accurate with the relative  $\ell_2$  error of  $2.48\% \pm 0.04\%$  over 100 test instances. Fig. 5 shows snapshots of one of the learned heat fields and the corresponding absolute error at  $t = 1.0$ . It can be seen that the errors are mainly at the domain boundary.

## 5.4 1D Burgers' Equation

In this experiment, we conduct experiments to simulate 1D periodic Burgers' equation defined as follows:

$$\frac{\partial u}{\partial t} = -u \frac{\partial u}{\partial x} + 0.01 \Delta u, \quad (18)$$

where  $x \in [0, 1]$ ,  $t \in [0, 1]$ .

The initial condition  $u_0$  is generated from the Gaussian random field  $\mathcal{N}(0, 625(-\Delta + 25I)^{-4})$  with periodic boundaries, which is in line with the setting in [54].

Apart from the Euler–Maruyama method [53], we also consider other numerical methods to simulate the random process in Eq. 6, including Runge–Kutta method [48] and Heun's method [53]. The detailed algorithms can be seen in Appendix C.2.4. As the results in Fig. 6, high-order numerical methods obtain more accurate simulation, and the mean relative error of the Runge–Kutta method over ten time steps is  $0.94\% \pm 0.10\%$ .

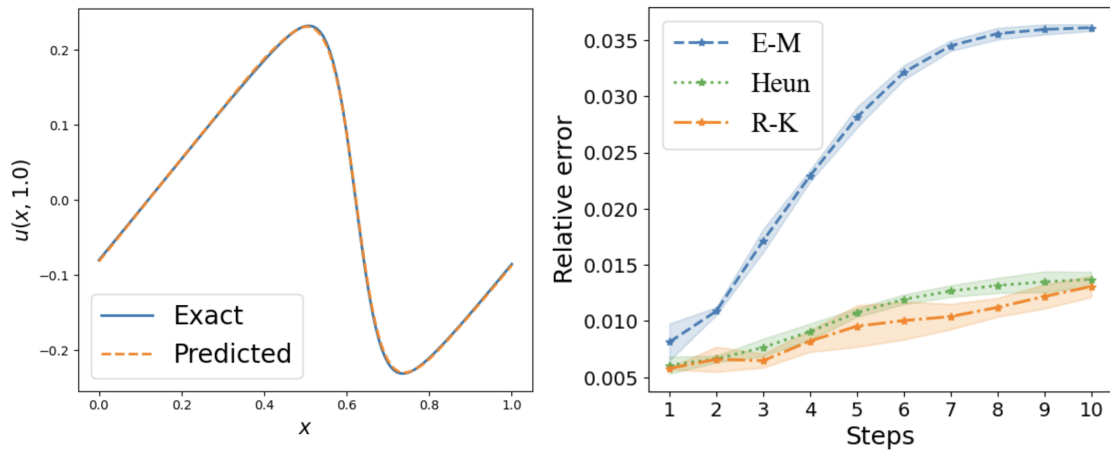


Figure 6: 1D Burgers' Equation. **Left:** The ground-truth solution versus the prediction of a learned MCNO (Runge–Kutta method) for an example in the test set at  $t = 1.0$ s. **Right:** Comparison of the relative error of each step with different simulating methods of BSDEs, including Euler–Maruyama (E-M), Runge–Kutta (R-K), and Heun's method.

## 6 Conclusion and Discussion

In this paper, we propose MCNO, which utilizes the Monte Carlo simulation to train diffusion-related PDEs in an unsupervised way. Both theoretical and experimental analyses reveal the ability of MCNO to adapt to complex spatial conditions and larger temporal steps when handling diffusion terms. This paper also has some limitations: (1) For the theoretical part, the gradient flow of the MCNO loss function requires further analyses; (2) When conducting the random walks for PDEs with Dirichlet boundary conditions, the temporal steps cannot be as large as the ones in periodic PDE due to the stop-time; (3) MCNO is trained on the fixed grid in the experiments, while it has potential to extend to the mesh-free scheme. Apart from addressing the limitations, we also propose other future studies: (1) Extend the proposed MCNO to broad scenarios, such

as high-dimensional PDEs and optimal control problems; (2) Utilize the techniques from out-of-distribution generalization [49] to improve the generalization ability of MCNO; (3) Combine the advantages of the Monte Carlo and other numerical methods. e.g., train neural operators in an Eulerian-Lagrangian regime [7].

## References

- [1] Deniz A Bezgin, Steffen J Schmidt, and Nikolaus A Adams. A data-driven physics-informed finite-volume scheme for nonclassical undercompressive shocks. *Journal of Computational Physics*, 437:110324, 2021.
- [2] James Bradbury, Roy Frostig, Peter Hawkins, Matthew James Johnson, Chris Leary, Dougal Maclaurin, George Necula, Adam Paszke, Jake VanderPlas, Skye Wanderman-Milne, and Qiao Zhang. JAX: composable transformations of Python+NumPy programs, 2018.
- [3] Johannes Brandstetter, Daniel E. Worrall, and Max Welling. Message passing neural PDE solvers. In *International Conference on Learning Representations*, 2022.
- [4] Shuhao Cao. Choose a transformer: Fourier or galerkin. In A. Beygelzimer, Y. Dauphin, P. Liang, and J. Wortman Vaughan, editors, *Advances in Neural Information Processing Systems*, 2021.
- [5] Zhao Chen, Yang Liu, and Hao Sun. Physics-informed learning of governing equations from scarce data. *Nature communications*, 12(1):1–13, 2021.
- [6] R Eugene Collins. Quantum mechanics as a classical diffusion process. *Foundations of Physics Letters*, 5(1):63–69, 1992.
- [7] G-H Cottet and Philippe Poncet. Advances in direct numerical simulations of 3d wall-bounded flows by vortex-in-cell methods. *Journal of computational physics*, 193(1):136–158, 2004.
- [8] Alex Damian, Tengyu Ma, and Jason D Lee. Label noise sgd provably prefers flat global minimizers. *Advances in Neural Information Processing Systems*, 34:27449–27461, 2021.
- [9] Adolf Fick. Ueber diffusion. *Annalen der Physik*, 170(1):59–86, 1855.
- [10] Jonathan Goodman. Convergence of the random vortex method. In *Hydrodynamic behavior and interacting particle systems*, pages 99–106. Springer, 1987.
- [11] Ling Guo, Hao Wu, Xiaochen Yu, and Tao Zhou. Monte carlo fpinns: Deep learning method for forward and inverse problems involving high dimensional fractional partial differential equations. *Computer Methods in Applied Mechanics and Engineering*, 400:115523, 2022.
- [12] Jiequn Han, Arnulf Jentzen, and Weinan E. Solving high-dimensional partial differential equations using deep learning. *Proceedings of the National Academy of Sciences*, 115(34):8505–8510, 2018.
- [13] Jihun Han, Mihai Nica, and Adam R Stinchcombe. A derivative-free method for solving elliptic partial differential equations with deep neural networks. *Journal of Computational Physics*, 419:109672, 2020.
- [14] Jan Hermann, Zeno Schätzle, and Frank Noé. Deep-neural-network solution of the electronic schrödinger equation. *Nature Chemistry*, 12(10):891–897, 2020.
- [15] Xiang Huang, Zhanhong Ye, Hongsheng Liu, Shi Bei Ji, Zidong Wang, Kang Yang, Yang Li, Min Wang, Haotian CHU, Fan Yu, Bei Hua, Lei Chen, and Bin Dong. Meta-auto-decoder for solving parametric partial differential equations. In Alice H. Oh, Alekh Agarwal, Danielle Belgrave, and Kyunghyun Cho, editors, *Advances in Neural Information Processing Systems*, 2022.

- [16] Xiaowei Jin, Shengze Cai, Hui Li, and George Em Karniadakis. Nsfnets (navier-stokes flow nets): Physics-informed neural networks for the incompressible navier-stokes equations. *Journal of Computational Physics*, 426:109951, 2021.
- [17] Matthias Karlbauer, Timothy Praditia, Sebastian Otte, Sergey Oladyshkin, Wolfgang Nowak, and Martin V Butz. Composing partial differential equations with physics-aware neural networks. In *International Conference on Machine Learning*, pages 10773–10801. PMLR, 2022.
- [18] George Em Karniadakis, Ioannis G Kevrekidis, Lu Lu, Paris Perdikaris, Sifan Wang, and Liu Yang. Physics-informed machine learning. *Nature Reviews Physics*, 3(6):422–440, 2021.
- [19] Diederik P. Kingma and Jimmy Ba. Adam: A method for stochastic optimization. In Yoshua Bengio and Yann LeCun, editors, *3rd International Conference on Learning Representations, ICLR 2015, San Diego, CA, USA, May 7-9, 2015, Conference Track Proceedings*, 2015.
- [20] Tomasz J Kozubowski, Mark M Meerschaert, and Krzysztof Podgorski. Fractional laplace motion. *Advances in applied probability*, 38(2):451–464, 2006.
- [21] Aditi Krishnapriyan, Amir Gholami, Shandian Zhe, Robert Kirby, and Michael W Mahoney. Characterizing possible failure modes in physics-informed neural networks. *Advances in Neural Information Processing Systems*, 34:26548–26560, 2021.
- [22] Stig Larsson and Vidar Thomée. *Partial differential equations with numerical methods*, volume 45. Springer, 2003.
- [23] Hong Li, Qilong Zhai, and Jeff ZY Chen. Neural-network-based multistate solver for a static schrödinger equation. *Physical Review A*, 103(3):032405, 2021.
- [24] Zijie Li, Kazem Meidani, and Amir Barati Farimani. Transformer for partial differential equations’ operator learning. *arXiv preprint arXiv:2205.13671*, 2022.
- [25] Zongyi Li, Daniel Zhengyu Huang, Burigede Liu, and Anima Anandkumar. Fourier neural operator with learned deformations for pdes on general geometries. *arXiv preprint arXiv:2207.05209*, 2022.
- [26] Zongyi Li, Nikola Kovachki, Kamyar Azizzadenesheli, Burigede Liu, Kaushik Bhattacharya, Andrew Stuart, and Anima Anandkumar. Neural operator: Graph kernel network for partial differential equations. *arXiv preprint arXiv:2003.03485*, 2020.
- [27] Zongyi Li, Nikola Borislavov Kovachki, Kamyar Azizzadenesheli, Burigede Liu, Kaushik Bhattacharya, Andrew M. Stuart, and Anima Anandkumar. Fourier neural operator for parametric partial differential equations. In *9th International Conference on Learning Representations, ICLR 2021, Virtual Event, Austria, May 3-7, 2021*. OpenReview.net, 2021.
- [28] Zongyi Li, Hongkai Zheng, Nikola Kovachki, David Jin, Haoxuan Chen, Burigede Liu, Kamyar Azizzadenesheli, and Anima Anandkumar. Physics-informed neural operator for learning partial differential equations. *arXiv preprint arXiv:2111.03794*, 2021.
- [29] Anna Lischke, Guofei Pang, Mamikon Gulian, Fangying Song, Christian Glusa, Xiaoning Zheng, Zhiping Mao, Wei Cai, Mark M Meerschaert, Mark Ainsworth, et al. What is the fractional laplacian? a comparative review with new results. *Journal of Computational Physics*, 404:109009, 2020.



- [30] Lu Lu, Pengzhan Jin, Guofei Pang, Zhongqiang Zhang, and George Em Karniadakis. Learning nonlinear operators via deepnet based on the universal approximation theorem of operators. *Nature Machine Intelligence*, 3(3):218–229, 2021.
- [31] A v Luikov. *Analytical heat diffusion theory*. Elsevier, 2012.
- [32] Xuerong Mao. *Stochastic differential equations and applications*. Elsevier, 2007.
- [33] Nils Margenberg, Dirk Hartmann, Christian Lessig, and Thomas Richter. A neural network multigrid solver for the navier-stokes equations. *Journal of Computational Physics*, 460:110983, 2022.
- [34] Revanth Matthey and Susanta Ghosh. A novel sequential method to train physics informed neural networks for allen cahn and cahn hilliard equations. *Computer Methods in Applied Mechanics and Engineering*, 390:114474, 2022.
- [35] Chloé Mimeau and Iraj Mortazavi. A review of vortex methods and their applications: From creation to recent advances. *Fluids*, 6(2):68, 2021.
- [36] Sebastian K Mitusch, Simon W Funke, and Miroslav Kuchta. Hybrid fem-nn models: Combining artificial neural networks with the finite element method. *Journal of Computational Physics*, 446:110651, 2021.
- [37] Guofei Pang, Lu Lu, and George Em Karniadakis. fpinns: Fractional physics-informed neural networks. *SIAM Journal on Scientific Computing*, 41(4):A2603–A2626, 2019.
- [38] Panos Pantidis and Mostafa E Mobasher. Integrated finite element neural network (i-fenn) for non-local continuum damage mechanics. *Computer Methods in Applied Mechanics and Engineering*, 404:115766, 2023.
- [39] Etienne Pardoux and Shige Peng. Backward stochastic differential equations and quasilinear parabolic partial differential equations. In *Stochastic partial differential equations and their applications*, pages 200–217. Springer, 1992.
- [40] Etienne Pardoux and Shanjian Tang. Forward-backward stochastic differential equations and quasilinear parabolic pdes. *Probability Theory and Related Fields*, 114(2):123–150, 1999.
- [41] Kevin Min Seong Park and Adam R Stinchcombe. Deep reinforcement learning of viscous incompressible flow. *Journal of Computational Physics*, 467:111455, 2022.
- [42] Adam Paszke, Sam Gross, Francisco Massa, Adam Lerer, James Bradbury, Gregory Chanan, Trevor Killeen, Zeming Lin, Natalia Gimelshein, Luca Antiga, et al. Pytorch: An imperative style, high-performance deep learning library. *Advances in neural information processing systems*, 32, 2019.
- [43] Olivier Pironneau. On the transport-diffusion algorithm and its applications to the navier-stokes equations. *Numerische Mathematik*, 38(3):309–332, 1982.
- [44] Maziar Raissi, Paris Perdikaris, and George E Karniadakis. Physics-informed neural networks: A deep learning framework for solving forward and inverse problems involving nonlinear partial differential equations. *Journal of Computational physics*, 378:686–707, 2019.
- [45] Maziar Raissi, Alireza Yazdani, and George Em Karniadakis. Hidden fluid mechanics: Learning velocity and pressure fields from flow visualizations. *Science*, 367(6481):1026–1030, 2020.

- [46] Lorenz Richter and Julius Berner. Robust sde-based variational formulations for solving linear pdes via deep learning. In *International Conference on Machine Learning*, pages 18649–18666. PMLR, 2022.
- [47] Lorenz Richter, Leon Sallandt, and Nikolas Nüsken. Solving high-dimensional parabolic pdes using the tensor train format. In *International Conference on Machine Learning*, pages 8998–9009. PMLR, 2021.
- [48] A. J. Roberts. Modify the improved euler scheme to integrate stochastic differential equations, 2012.
- [49] Zheyang Shen, Jiashuo Liu, Yue He, Xingxuan Zhang, Renzhe Xu, Han Yu, and Peng Cui. Towards out-of-distribution generalization: A survey. *arXiv preprint arXiv:2108.13624*, 2021.
- [50] Arthur S Sherman and Charles S Peskin. A monte carlo method for scalar reaction diffusion equations. *SIAM journal on scientific and statistical computing*, 7(4):1360–1372, 1986.
- [51] Wenlei Shi, Xinquan Huang, Xiaotian Gao, Xinran Wei, Jia Zhang, Jiang Bian, Mao Yang, and Tie-Yan Liu. Lordnet: Learning to solve parametric partial differential equations without simulated data. *arXiv preprint arXiv:2206.09418*, 2022.
- [52] Pauli Virtanen, Ralf Gommers, Travis E Oliphant, Matt Haberland, Tyler Reddy, David Cournapeau, Evgeni Burovski, Pearu Peterson, Warren Weckesser, Jonathan Bright, et al. Scipy 1.0: fundamental algorithms for scientific computing in python. *Nature methods*, 17(3):261–272, 2020.
- [53] J. Vom Scheidt. Kloeden, p. e.; platen, e., numerical solution of stochastic differential equations. berlin etc., springer-verlag 1992. xxxvi, 632 pp., 85 figs., dm 118,00. isbn 3-540-54062-8 (applications of mathematics 23). *ZAMM - Journal of Applied Mathematics and Mechanics / Zeitschrift für Angewandte Mathematik und Mechanik*, 74(8):332–332, 1994.
- [54] Sifan Wang, Hanwen Wang, and Paris Perdikaris. Learning the solution operator of parametric partial differential equations with physics-informed deepnets. *Science advances*, 7(40):eabi8605, 2021.
- [55] Sifan Wang, Xinling Yu, and Paris Perdikaris. When and why pinns fail to train: A neural tangent kernel perspective. *Journal of Computational Physics*, 449:110768, 2022.
- [56] Yizheng Wang, Jia Sun, Wei Li, Zaiyuan Lu, and Yinghua Liu. Cenn: Conservative energy method based on neural networks with subdomains for solving variational problems involving heterogeneous and complex geometries. *Computer Methods in Applied Mechanics and Engineering*, 400:115491, 2022.
- [57] Li-Ming Yang. Kinetic theory of diffusion in gases and liquids. i. diffusion and the brownian motion. *Proceedings of the Royal Society of London. Series A, Mathematical and Physical Sciences*, pages 94–116, 1949.
- [58] Rui Zhang, Peiyan Hu, Qi Meng, Yue Wang, Rongchan Zhu, Bingguang Chen, Zhi-Ming Ma, and Tie-Yan Liu. Drvn (deep random vortex network): A new physics-informed machine learning method for simulating and inferring incompressible fluid flows. *Physics of Fluids*, 34(10):107112, 2022.

- [59] Xicheng Zhang. Stochastic functional differential equations driven by lévy processes and quasi-linear partial integro-differential equations. *The Annals of Applied Probability*, 22(6):2505–2538, 2012.
- [60] Xicheng Zhang. Stochastic lagrangian particle approach to fractal navier-stokes equations. *Communications in Mathematical Physics*, 311(1):133–155, 2012.
- [61] Qingqing Zhao, David B. Lindell, and Gordon Wetzstein. Learning to solve pde-constrained inverse problems with graph networks. In *ICML*, 2022.
- [62] David Zwicker. py-pde: A python package for solving partial differential equations. *Journal of Open Source Software*, 5(48):2158, 2020.

## A Algorithm

---

### Algorithm 1: Monte Carlo Neural Operator

---

**Input:** Distribution of initial states  $\mathcal{D}_0$ , neural operator  $\mathcal{G}_\theta$ , and the coordinates of the fixed grids  $\{\mathbf{x}_p\}_{p=1}^P$

- 1 **for**  $E$  epochs **do**
- 2     Sample  $B$  initial states  $\{u_0^b\}_{b=1}^B$  uniformly from  $\mathcal{D}_0$ ;
- 3     **while**  $t \leq T$  **do**
- 4         Let  $t = 0$ ,  $\mathcal{L}_{\text{MCNO}} = 0$ , and  $u_t^b = u_0^b$  for all  $b \in \{1, \dots, B\}$ ;
- 5         Utilize Fourier transform to interpolate the grid of  $u_t^b$  to the high resolution one  $\hat{u}_t^b$ ;
- 6         Sample  $M$  trajectories starting from each grid  $\mathbf{x}_p$  ;
- 7          $\mathbf{x}_{p,m}^b = \mathbf{x}_p - \beta[u](\mathbf{x}, t + \Delta t)\Delta t - \sqrt{2\kappa}\Delta\mathbf{B}_m$ ;
- 8         Approximate  $u_{t+\Delta t}^b$  via the average of  $M$  trajectories :  
 $u_{t+\Delta t}^{\text{MC},b}(\mathbf{x}_p) = \frac{1}{M} \sum_{m=1}^M \hat{u}_t^b(\mathbf{x}_{p,m}^b) + f(\mathbf{x}_p, t + \Delta t)\Delta t$ ;
- 9         Calculate the prediction given by neural operator  $\mathcal{G}_\theta$ :  
 $u_{t+\Delta t}^{\text{NO},b}(\mathbf{x}_p) = \mathcal{G}_\theta(u_0^b, t + \Delta t)(\mathbf{x}_p)$ ;
- 10         Update the loss function  $\mathcal{L}_{\text{MCNO}}$ :  
 $\mathcal{L}_{\text{MCNO}} = \mathcal{L}_{\text{MCNO}} + \sum_{b=1}^B \sum_{p=1}^P \left\| u_{t+\Delta t}^{\text{NO},b}(\mathbf{x}_p) - u_{t+\Delta t}^{\text{MC},b}(\mathbf{x}_p) \right\|_2^2$ ;
- 11         Update  $u_t^b$  and  $t$ :  $u_t^b = \mathcal{G}_\theta(u_0^b, t + \Delta t)$  and  $t = t + \Delta t$ ;
- 12     Update  $\mathcal{G}_\theta$ 's parameters:  $\theta = \text{optim. Adam}(\theta, \nabla_\theta \mathcal{L}_{\text{MCNO}})$ ;

---

## B Theory

In this section, we study some theoretical properties of MCNO when handling the diffusion term. In detail, we consider the periodical diffusion equation defined as follows:

$$\frac{\partial u}{\partial t} = \kappa \Delta u, \quad x \in [0, 2\pi], t \in [0, T]. \quad (19)$$

**Theorem B.1.** Let  $u_t(x)$  be the diffusion equation in the form of Eq. 19,  $u_{t+\Delta t}^{\text{FDM}}(x)$  and  $u_{t+\Delta t}^{\text{MCM}}(x)$  denote the one-step label starting from  $u_t(x)$ , given by FDM and MCM, respectively. Assume  $\Delta_t u$  and  $u_t(x)$  are Lipschitz functions with respect to  $t$  and  $x$ , respectively, i.e.:

$$|\Delta_{t_1} u(x) - \Delta_{t_2} u(x)| \leq L_{\Delta u}^t |t_1 - t_2|, \quad |u_t(x_1) - u_t(x_2)| \leq L_u^x |x_1 - x_2|. \quad (20)$$

Then, we have

- 1)  $|u_{t+\Delta t}^{\text{FDM}}(x) - u_{t+\Delta t}(x)| \leq \frac{\kappa L_{\Delta u}^t \Delta t^2}{2}$ ;
- 2)  $|u_{t+\Delta t}^{\text{MCM}}(x) - u_{t+\Delta t}(x)| \leq \epsilon$  holds with probability at least  $1 - \frac{(2L_u^x)^2 \kappa \Delta t}{M\epsilon^2}$ .

*Proof of Theorem B.1.* Firstly, we give the upper bound of  $|u_{t+\Delta t}^{\text{FDM}}(x) - u_{t+\Delta t}(x)|$  as follows:

$$\begin{aligned}
|u_{t+\Delta t}^{\text{FDM}}(x) - u_{t+\Delta t}(x)| &= \left| u_t(x) + \kappa \int_t^{t+\Delta t} \Delta u_s(x) ds - [u_t(x) + \Delta u_t(x)\Delta t] \right| \\
&= \left| \kappa \int_t^{t+\Delta t} (\Delta u_s(x) - \Delta u_t(x)) ds \right| \\
&\leq \kappa L_{\Delta u}^t \int_t^{t+\Delta t} (s-t) ds \\
&= \frac{\kappa L_{\Delta u}^t \Delta t^2}{2}.
\end{aligned} \tag{21}$$

The one-step label constructed by MCM can be written as follows:

$$u_{t+\Delta t}^{\text{MCM}}(x) = \frac{1}{M} \sum_{m=1}^M u_t(\hat{x}_m), \quad \hat{x}_m = x - \sqrt{2\kappa\Delta t}z_m, \quad z_m \sim \mathcal{N}(0, 1), \tag{22}$$

where  $M$  denotes the number of particles sampled in MCM. According to the probabilistic representation of Eq. 19, we have  $u_{t+\Delta t}(x) = \mathbb{E}_m[u_t(\hat{x}_m)]$ , which implies that  $u_{t+\Delta t}^{\text{MCM}}(x)$  is an unbiased estimator of  $u_{t+\Delta t}(x)$ , i.e.,  $\mathbb{E}[u_{t+\Delta t}^{\text{MCM}}(x) - u_{t+\Delta t}(x)] = 0$ . Furthermore, the variance of  $u_{t+\Delta t}^{\text{MCM}}(x)$  can be bounded as follows:

$$\begin{aligned}
\text{Var}[u_{t+\Delta t}^{\text{MCM}}] &= \text{Var}\left[\frac{1}{M} \sum_{m=1}^M u_t(x - \sqrt{2\kappa\Delta t}z_m)\right] \\
&= \frac{1}{M} \text{Var}[u_t(x - \sqrt{2\kappa\Delta t}z)] \\
&\leq \frac{1}{M} 2(L_u^x)^2 \text{Var}[\sqrt{2\kappa\Delta t}z] \\
&= \frac{(2L_u^x)^2 \kappa \Delta t}{M}.
\end{aligned} \tag{23}$$

Thus, according to the Chebyshev's inequality, we have  $|u_{t+\Delta t}^{\text{MCM}}(x) - u_{t+\Delta t}(x)| \leq \epsilon$  with probability at least  $1 - \frac{(2L_u^x)^2 \kappa \Delta t}{M\epsilon^2}$  for any  $\epsilon > 0$ .  $\square$

**Theorem B.2.** Let  $u_t(x)$  be the diffusion equation in the form of Eq. 19, and assume the exact solution can be written as:  $u_t(x) = \sum_{n=1}^N \sin(nx)\phi_n(t)$ . Let  $\mathcal{G}_\theta$  be the neural operator, and its prediction on  $u_t(x)$  can be written as  $\mathcal{G}_\theta(u_0, t)(x) = \sum_{n=1}^N \sin(nx)(\phi_n(t) + r_n)$ , where  $r_n$  denotes the residual of coefficient on each Fourier basis. Let  $u_{t+\Delta t}^{\text{FDM}}(x)$  and  $u_{t+\Delta t}^{\text{MCM}}(x)$  denote the one-step label starting from  $\mathcal{G}_\theta(u_0, t)(x)$ , given by FDM and MCM, respectively. Then, we have

- 1)  $|u_{t+\Delta t}^{\text{FDM}}(x) - u_{t+\Delta t}(x)| \leq \sum_{n=1}^N |r_n(\kappa n^2 \Delta t - 1)| + o(\Delta t)$ ;
- 2)  $|u_{t+\Delta t}^{\text{MCM}}(x) - u_{t+\Delta t}(x)| \leq \sum_{n=1}^N |r_n| + \epsilon$  holds with probability at least  $1 - 2 \exp\left(-\frac{\epsilon^2 M}{2(\sum_{n=1}^N |\phi_n(t)|)^2}\right)$ .

*Proof of Theorem B.2.* Firstly, we give the upper bound of  $|u_{t+\Delta t}^{\text{FDM}}(x) - u_{t+\Delta t}(x)|$  as follows:

$$\begin{aligned}
& |u_{t+\Delta t}^{\text{FDM}}(x) - u_{t+\Delta t}(x)| \\
&= \left| \mathcal{G}_\theta(u_0, t)(x) + \kappa \Delta t \frac{\partial^2 \mathcal{G}_\theta(u_0, t)(x)}{\partial x^2} - [u_t(x) + \Delta u_t(x) \Delta t + o(\Delta t)] \right| \\
&= \left| \sum_{n=1}^N \sin(nx) (\phi_n(t) + r_n) (1 - \kappa \Delta t n^2) - \sum_{n=1}^N \sin(nx) \phi_n(t) (1 - \kappa \Delta t n^2) + o(\Delta t) \right| \\
&= \left| \sum_{n=1}^N \sin(nx) r_n (1 - \kappa \Delta t n^2) + o(\Delta t) \right| \\
&\leq \sum_{n=1}^N |r_n (\kappa n^2 \Delta t - 1)| + o(\Delta t)
\end{aligned} \tag{24}$$

The one-step label constructed by MCM can be written as follows:

$$u_{t+\Delta t}^{\text{MCM}}(x) = \frac{1}{M} \sum_{m=1}^M \mathcal{G}_\theta(u_0, t)(x - \sqrt{2\kappa \Delta t} z_m), \quad z_m \sim \mathcal{N}(0, 1), \tag{25}$$

where  $M$  denotes the number of particles sampled in MCM. According to the Hoeffding's inequality, we have

$$\mathbb{P} \left( \left| \sum_{m=1}^M \frac{1}{M} u_t(x - \sqrt{2\kappa \Delta t} z_m) - \mathbb{E}_z[u_t(x - \sqrt{2\kappa \Delta t} z)] \right| \leq \epsilon \right) \leq 1 - 2 \exp \left( - \frac{\epsilon^2 M}{2(\sum_{n=1}^N |\phi_n(t)|)^2} \right) \tag{26}$$

Thus, we can obtain upper bound of  $\mathbb{E}_z[|u_{t+\Delta t}^{\text{MCM}}(x) - u_{t+\Delta t}(x)|]$  with probability at least  $1 - 2 \exp \left( - \frac{\epsilon^2 M}{2(\sum_{n=1}^N |\phi_n(t)|)^2} \right)$  as follows:

$$\begin{aligned}
& |u_{t+\Delta t}^{\text{MCM}}(x) - u_{t+\Delta t}(x)| \\
&= \left| \frac{1}{M} \sum_{m=1}^M [\mathcal{G}(u_0)(x - \sqrt{2\kappa \Delta t} z_m, t) - u_t(x - \sqrt{2\kappa \Delta t} z_m)] + \left[ \sum_{m=1}^M \frac{1}{M} u_t(x - \sqrt{2\kappa \Delta t} z_m) - \mathbb{E}_z[u_t(x - \sqrt{2\kappa \Delta t} z)] \right] \right| \\
&\leq \left| \frac{1}{M} \sum_{m=1}^M \sum_{n=1}^N \sin(n(x - \sqrt{2\kappa \Delta t} z_m)) [\phi_n(t) + r_n - \phi_n(t)] \right| + \left| \sum_{m=1}^M \frac{1}{M} u_t(x - \sqrt{2\kappa \Delta t} z_m) - \mathbb{E}_z[u_t(x - \sqrt{2\kappa \Delta t} z)] \right| \\
&= \mathbb{E}_z \left[ \left| \sum_{n=1}^N \sin(n(x - \sqrt{2\kappa \Delta t} z_m)) [\phi_n(t) + r_n - \phi_n(t)] \right| \right] + \epsilon \\
&= \mathbb{E}_z \left[ \left| \sum_{n=1}^N \sin(n(x - \sqrt{2\kappa \Delta t} z_m)) r_n \right| \right] + \epsilon \\
&\leq \sum_{n=1}^N |r_n| + \epsilon.
\end{aligned} \tag{27}$$

□

## B.1 Additional Analyses about the Theoretical Results

In this section, we consider the PDE with linear term given by the Laplacian operator defined as follows:

$$\frac{\partial u}{\partial t} = \beta[u](\mathbf{x}, t) \cdot \nabla u + \kappa \Delta u, \tag{28}$$

$$u(\mathbf{x}, 0) = u_0(\mathbf{x}). \quad (29)$$

- Note that when  $\beta$  is a fixed constant, i.e., the Eq. 28 degenerates into the convection-diffusion equation, MCM still provides an unbiased estimator for the operator learning algorithm. Thus, the training target of MCM is more accurate than the one of FDM when  $\beta$  is a constant or with small temporal and spatial variation.
- When  $\beta$  is not a constant, the error of one step roll-out of FDM and MCM are both  $o(\Delta t^2)$  [53]. Moreover, we can also utilize the Eulerian-Lagrangian method (e.g. Vortex-in-Cell [7]), which combines the advantages of the Eulerian and Lagrangian methods, respectively. We regard this expansion as an important future work.

## C Implementation Details and Supplementary Experiments

### C.1 Baselines

In this paper, we adopt two unsupervised neural operator learning method, including:

**PI-DeepONet** [54] PI-DeepONet utilized the PDE residuals to train DeepONets in an unsupervised way. The loss function in PI-DeepONet can be formulated as follows:

$$\begin{aligned} \mathcal{L}_{\text{PI-DeepONet}} &= \mathcal{L}_{\text{operator}} + \mathcal{L}_{\text{physics}}, \\ \text{where } \mathcal{L}_{\text{operator}} &= \text{MSE}[\mathcal{G}_\theta(u_0^b, t=0)(\mathbf{x}_p) - \mathcal{G}(u_0^b, t=0)(\mathbf{x}_p)], \\ \mathcal{L}_{\text{physics}} &= \text{MSE}[\mathcal{R}(\mathcal{G}_\theta(u_0^b, t)(\mathbf{x}_p), \mathbf{x}_p, t)], \end{aligned} \quad (30)$$

where MSE represents the mean square error,  $\mathcal{G}_\theta$  represents a neural operator,  $\mathcal{G}$  and  $\mathcal{R}$  denote the ground-truth and the residual of the PDE operator, respectively. As shown in Eq. 30,  $\mathcal{L}_{\text{operator}}$  and  $\mathcal{L}_{\text{physics}}$  enforce  $\mathcal{G}_\theta$  to satisfy the initial conditions (or boundary conditions) and the PDE constraints, respectively. Like PINNs [44], the PDE residuals in Eq. 30 are calculated via the auto-differentiation.

**PINO** [28] PINO utilized the FDM to construct the loss function between  $\mathcal{G}_\theta(u_t^b)$  and  $\mathcal{G}_\theta(u_{t+\Delta t}^b)$ , and PINO utilized the FNO [23] as the backbone network. The loss function in PINO can be formulated as follows:

$$\begin{aligned} \mathcal{L}_{\text{PINO}} &= \mathcal{L}_{\text{operator}} + \alpha \mathcal{L}_{\text{physics}}, \\ \text{where } \mathcal{L}_{\text{operator}} &= \text{MSE}[\mathcal{G}_\theta(u_0^b, t=0)(\mathbf{x}_p) - \mathcal{G}(u_0^b, t=0)(\mathbf{x}_p)], \\ \mathcal{L}_{\text{physics}} &= \sum_{t=0}^{T-\Delta t} \text{MSE}[\mathcal{G}_\theta(u_0^b, t+\Delta t)(\mathbf{x}_p) - \mathcal{G}_\theta(u_0^b, t)(\mathbf{x}_p) - \mathcal{F}(\mathcal{G}_\theta, \mathbf{x}_p, t)], \end{aligned} \quad (31)$$

where  $\mathcal{F}$  denotes the update regime of FDM. Note that despite the temporal discretization in PINO is based on FDM, the spatial derivative is calculated via Fourier transform.

### C.2 Implementation Details

In this paper, We adopt Pytorch [42] to implement MCNO and PINO, and JAX [2] for PI-DeepONet, respectively.

### C.2.1 1D Diffusion Equation

For MCNO, we utilize the 4-layer 1D FNO as the backbone network, with  $width = 20$ ,  $mode = 20$  and GeLU activation. We utilize Adam to optimize the neural operator for 10000 epochs with the initial learning rate 0.01, and decay the learning rate by a factor of 0.5 every 500 epochs. For each epoch, we sample 1024 initial conditions from  $\mathcal{D}_0$  and 128 particles to simulate the BSDEs. For PINO, we utilize 4-layer 2D FNO as the backbone network, with  $width = 32$ ,  $mode = 20$  and GeLU activation. For  $\alpha$  in the loss function Eq. 31, we choose the best  $\alpha$  in  $\{0.1, 0.5, 1.0, 2.0\}$ , and other setups are in line with MCNO. For PI-DeepONet, we choose the hyper-parameters in line with the paper in [54], and extend the training iterations to 10000 to make sure the convergence of the model.

Furthermore, there is no GPU package for the Lévy sampling as far as we know. Thus, we utilize the code `scipy.stats.levy_stable` [52] to generate the corresponding random processes. Moreover, the generation of Lévy sampling is ten times slower than Gaussian sampling on CPU, and even though the efficiency of Lévy sampling is the same as Gaussian on GPU, MCNO still has 20x speedup compared with MCM.

### C.2.2 2D Navier-Stokes Equation

For data generation, we utilize Pseudo-Spectral Method (PSM) to generate the ground truth test data with the time-step of  $10^{-4}$  for the Crank–Nicolson scheme. Furthermore, all PDE instances are generated on the grid  $256 \times 256$ , then downsampled to  $64 \times 64$ , which is in line with the setting in [23].

For MCNO, we utilize the 4-layer 2D FNO as the backbone network, with  $width = 24$ ,  $mode = 16$  and GeLU activation. We utilize Adam to optimize the neural operator for 10000 epochs with the initial learning rate 0.001, and decay the learning rate by a factor of 0.5 every 2000 epochs. For each epoch, we sample 128 initial conditions from  $\mathcal{D}_0$  and 32 particles to simulate the BSDEs. For PINO, we use the same network in line with the ones in MCNO. We utilize Adam to optimize the neural operator for 20000 epochs with the initial learning rate 0.001, and decay the learning rate by a factor of 0.5 every 2000 epochs. For each epoch, we sample 64 initial conditions from  $\mathcal{D}_0$  due to the memory limitation. For  $\alpha$  in the loss function Eq. 31, we choose the best  $\alpha$  in  $\{0.1, 0.5, 1.0, 2.0\}$ .

### C.2.3 Heat Diffusion on a Circular Ring

The ground-truth data is generated via the Python package ‘py-pde’ [62], and the step size is fixed as  $10^{-4}$ . We conduct MCNO to simulate corresponding heat equations and fix the step size as 20. The initial heat distribution is generated from  $u_0 \sim \mathcal{N}(0, 3^{3/2}(-\Delta + 9I)^{-1})$ , and the width of the ring is divided into 128 lattices.

In this experiment, we utilize the 4-layer 1D FNO as the backbone network, with  $width = 20$ ,  $mode = 12$  and GeLU activation. We utilize Adam to optimize the neural operator for 5000 epochs with the initial learning rate 0.01, and decay the learning rate by a factor of 0.5 every 500 epochs. For each epoch, we sample 1024 initial conditions from  $\mathcal{D}_0$  and 128 particles to simulate the BSDEs.

### C.2.4 1D Burgers’ Equation

For Burgers’ Equation, we divide the spatial and temporal domains into 128 and 10 grid elements, respectively.



We utilize the 4-layer 1D FNO as the backbone network, with  $width = 64$ ,  $mode = 12$  and GeLU activation. We utilize Adam to optimize the neural operator for 10000 epochs with the initial learning rate 0.0005, and decay the learning rate by a factor of 0.5 every 1000 epochs. For each epoch, we sample 512 initial conditions from  $\mathcal{D}_0$  and 128 particles to simulate the BSDEs.

Furthermore, the form of the Runge–Kutta method is given as follows:

$$\begin{aligned} d\mathbf{x}_m^1 &= -\beta[u](\mathbf{x}, t + \Delta t)\Delta t - \sqrt{2\kappa\Delta t}(\mathbf{z}_m - \mathbf{s}_m); \\ d\mathbf{x}_m^2 &= -\beta[u](\mathbf{x} + d\mathbf{x}_m^1, t)\Delta t - \sqrt{2\kappa\Delta t}(\mathbf{z}_m + \mathbf{s}_m); \\ \mathbf{x}_m &= \mathbf{x} + \frac{1}{2}(d\mathbf{x}_m^1 + d\mathbf{x}_m^2), \end{aligned} \quad (32)$$

where  $\mathbf{z}_m$  and  $\mathbf{s}_m$  denote the standard Gaussian distribution and uniform distribution over  $\{\pm 1\}$ . Furthermore, the Heun’s method is given as follows:

$$\begin{aligned} d\mathbf{x}_m^1 &= -\beta[u](\mathbf{x}, t + \Delta t)\Delta t - \sqrt{2\kappa\Delta t}\mathbf{z}_m; \\ d\mathbf{x}_m^2 &= -\beta[u](\mathbf{x} + d\mathbf{x}_m^1, t)\Delta t; \\ \mathbf{x}_m &= \mathbf{x} + \frac{1}{2}(d\mathbf{x}_m^1 + d\mathbf{x}_m^2) - \sqrt{2\kappa\Delta t}\mathbf{z}_m. \end{aligned} \quad (33)$$

### C.3 Ablation Experiments

In this section, we conduct ablation experiments to reveal the effects of the number of sampling and Fourier Interpolation (FI) methods when training MCNO on the diffusion equation for long-time simulation. The basic settings align with the experiments in Sec. 5.1.2. We set the number of sampling as  $\{32, 64, 128, 256\}$  to train MCNO, respectively. When the number of sampling  $M > 128$ , the performances of MCNO persist almost unchanged, which reveals that the training of MCNO is relatively robust to the number of sampling (on the left side of Fig. 7). Furthermore, we test the effects of the FI trick on the right side of Fig. 7, and the results indicate that the FI trick plays an essential role in improving the precision of MCNO, especially for the task  $\kappa = 10^{-3}$ .

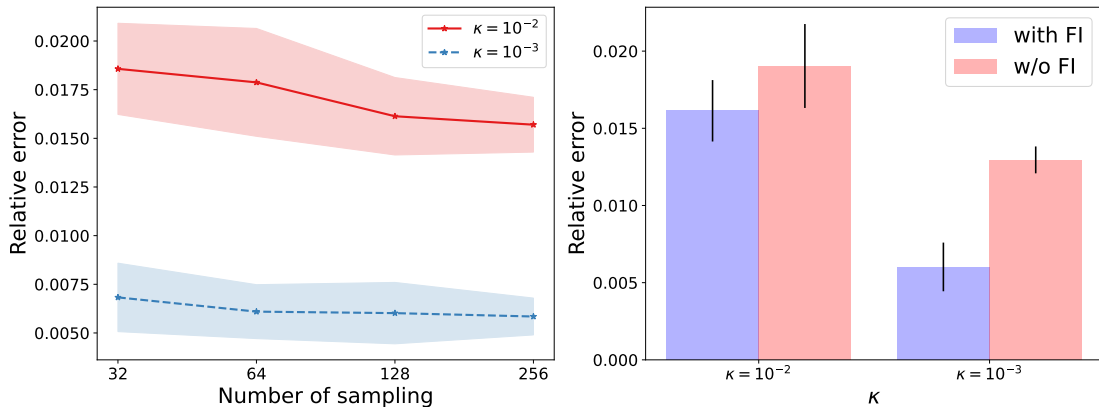


Figure 7: Ablation experiments on the diffusion equations for long temporal simulation. **Left:** Comparison of the relative error with different number of sampling when training MCNO. **Right:** The effects of FI with different  $\kappa$ .